Check for updates

View Article Online
View Journal

Journal of
Materials Chemistry A

Materials for energy and sustainability

Accepted Manuscript

This article can be cited before page numbers have been issued, to do this please use: C. Tougne, M. Daoudi, E. Ferri, V. H. Mareau, V. Dufaud, C. Santini, E. Espuche, O. Lottin, J. Perrin, J. Dillet, A. El Kaddouri, L. Porcar, L. GONON and H. Mendil-Jakani, *J. Mater. Chem. A*, 2026, DOI: 10.1039/D6TA03128E.

This is an Accepted Manuscript, which has been through the Royal Society of Chemistry peer review process and has been accepted for publication.

Accepted Manuscripts are published online shortly after acceptance, before technical editing, formatting and proof reading. Using this free service, authors can make their results available to the community, in citable form, before we publish the edited article. We will replace this Accepted Manuscript with the edited and formatted Advance Article as soon as it is available.

You can find more information about Accepted Manuscripts in the Information for Authors.

Please note that technical editing may introduce minor changes to the text and/or graphics, which may alter content. The journal's standard Terms & Conditions and the Ethical guidelines still apply. In no event shall the Royal Society of Chemistry be held responsible for any errors or omissions in this Accepted Manuscript or any consequences arising from the use of any information it contains.

ROYAL SOCIETY OF CHEMISTRY

rsc.li/materials-a

View Article Online
DOI: 10.1039/D6TA03128E

Revealing nanostructure-driven oxidative protection in thiourea-functionalized sPEEK hybrid membranes for PEM Fuel Cells

Claire Tougne[1], Meriem Daoudi[2], Evelise Ferri[3,4], Vincent H. Mareau[1], Véronique Dufaud[3], Catherine Santini[3], Eliane Espuche[4], Olivier Lottin[2], Jean-Christophe Perrin[2], Jérôme Dillet[2], Assma El Kaddouri[2], Lionel Porcar[5], Laurent Gonon[1*] and Hakima Mendil-Jakani[1*]

[1] *Université Grenoble Alpes, CEA, CNRS, Grenoble INP - UGA, IRIG, SyMMES, 38000 Grenoble, France*

[2] *Université de Lorraine, CNRS, LEMTA, 54000 Nancy, France.*

[3] *Université Lyon 1, CPE Lyon, CNRS, UMR 5128, Catalysis, Polymerization, processes and Materials (CP2M), 43 Bd du 11 novembre 1918, F-69616 Villeurbanne cedex, France.*

[4] *Université Claude Bernard Lyon 1, CNRS, UMR 5223, Ingénierie des Matériaux Polymères, INSA Lyon, Université Jean Monnet, F-69622 Villeurbanne Cedex, France.*

[5] *Institut Laue-Langevin, 38000 Grenoble, France*

** Corresponding authors:*

laurent.gonon@univ-grenoble-alpes.fr

hakima.mendil-jakani@cea.fr

Open Access Article. Published on 11 June 2026. Downloaded on 6/12/2026 10:57:08 PM.
This article is licensed under a Creative Commons Attribution 3.0 Unported Licence.

Journal of Materials Chemistry A Accepted Manuscript

ABSTRACT

Achieving long-term oxidative stability in proton exchange membrane fuel cells (PEMFCs) remains a major challenge. Here, we investigate the morphological mechanisms underlying the oxidative stability of thiourea-functionalized sol–gel (SG)/sulfonated poly(ether ether ketone) (sPEEK) hybrid membranes, previously developed using two organosilane precursors, N,N′-bis[3-(triethoxysilyl)propyl] thiourea (HTU) and N-phenyl,N′-[3-(triethoxysilyl)propyl] thiourea (TTU). These thiourea groups, introduced as sacrificial antioxidants, are used to tune the nanoscale organization of the SG phase within the polymer matrix. Contrast-variation small-angle neutron scattering (CV-SANS) shows that the SG phase is distributed within ionic nanochannels and interbundle regions. Although TEM and AFM indicate homogeneous dispersion at the microscale, sub-resolution fluctuations likely account for the SANS signal. HTU forms well-defined spherical hybrid domains (~5-6 nm), whereas TTU produces larger, less organized structures (~18-22 nm). Under oxidative conditions, pristine sPEEK swells and

View Article Online
DOI: 10.1039/D6TA03128E

degrades above 0.1 wt%, while hybrid membranes preserve structural integrity and conductivity up to 0.3 wt%. Hybrid membranes retain conductivity as long as SG within ionic domains is preserved; its consumption triggers secondary protection via SG in interbundle regions. This two-stage mechanism governs membrane integrity and proton transport under oxidative stress.

Keywords: Thiourea-functionalized hybrid membranes, Proton exchange membrane fuel cells; nanoscale morphology; small-angle neutron scattering; oxidative stability; durability

Highlights:

- Multiscale organization of SG nanophase across ionic and interbundle regions.
- Spatial localization enables decoupling of thiourea antioxidant reactivity.
- SG nanophase templating controls antioxidant accessibility and protection efficiency.
- Preferential thiourea oxidation stabilizes the sPEEK backbone.
- Nanostructure governs the conductivity-durability trade-off.

1. INTRODUCTION

The polymer electrolyte membrane (PEM) is a key component of proton exchange membrane fuel cells (PEMFCs), which convert hydrogen and oxygen into electricity with high efficiency and zero emissions. Serving as a selective barrier, the membrane conducts protons from anode to cathode while preventing gas crossover and short circuits, thereby ensuring both performance and operational safety. For heavy-duty applications such as buses and trucks, ambitious 2030 targets require operational lifetimes exceeding 30,000 hours.[1,2] Meeting these targets demands PEMs with high proton conductivity, low gas permeability, and outstanding thermal and mechanical stability under harsh conditions, including elevated temperatures (100–150 °C) and low relative humidity.

Despite significant progress, current PEMs struggle under such conditions. Even state-of-the-art perfluorinated membranes rapidly lose thermomechanical integrity and proton conductivity[3–5], resulting in premature system failure.[6–9] This highlights the urgent need for novel PEM materials and strategies to improve durability.

Several approaches have been explored, including interpenetrating networks[10–12] block copolymers[13–16] and polyaromatic membranes such as sPEEK.[17] Recent advances in nonfluorinated PEMs, ionogel-based PEMs, and composite membrane electrode assemblies have been comprehensively reviewed, particularly regarding proton transport, high-temperature operation, and hybrid architectures incorporating inorganic frameworks.[18–20] However, improving one property often compromises another, and no single approach has yet achieved the required balance. Since the early 2000's, fillers and reinforcements have been incorporated to enhance physical properties[21,22] while chemical stabilizers have been introduced to mitigate oxidative degradation.[23]

Open Access Article. Published on 11 June 2026. Downloaded on 6/12/2026 10:57:08 PM.
This article is licensed under a Creative Commons Attribution 3.0 Unported Licence.

Journal of Materials Chemistry A Accepted Manuscript

View Article Online
DOI: 10.1039/D6TA03128E

Open Access Article. Published on 11 June 2026. Downloaded on 6/12/2026 10:57:08 PM.
This article is licensed under a Creative Commons Attribution 3.0 Unported Licence.

Journal of Materials Chemistry A Accepted Manuscript

Two main stabilization strategies dominate the field. The first relies on inorganic additives, such as Ce(III), Mn(II), or their oxides nanoparticles, which scavenge harmful radicals.

This approach, however, suffers from sulfonic acid neutralisation, additives leaching, and dispersion challenges.[7,8,23–53] The second relies on organic sacrificial antioxidants, such as phenolic compounds or hydrogen peroxide reducers, which can be effective but often leach out unless covalently attached.[7,8,21,23,45–47,54–71] Moreover, conventional incorporation methods, such as solution casting, may disrupt membrane nanostructure and leave solvent residues.[43,72]

Recent studies on aromatic PEMs have also shown that nanostructured hybrid interfaces and acid-base interactions can improve both membrane stability and proton transport by promoting more continuous proton-conduction pathways and reinforcing the polymer network.[73–75]

An alternative approach is the impregnation of a nanostructured membrane with SG precursors, followed by *in situ* condensation into a 2D or 3D SG phase within the membrane.[72,76–79]

This strategy is solvent-compatible with various ionomers and enables the introduction of stabilizing phases.

Within this framework, the sPEEK matrix exhibits a hierarchical ionic morphology characterized by a typical ionomer-type nanophase separation between polymer aggregates and ionic domains, giving rise to a well-defined ionomer peak. In this context, sPEEK-rich "bundles" correspond to correlated polymer-rich regions surrounded by ionic domains, while "interbundle" regions refer to the entangled ionic matrix separating these bundles and defining the characteristic inter-domain spacing. [80,81]

The bundle organization is reflected in the low-q upturn of the scattering intensity (**Fig. S1a**), whereas higher-q features are associated with the characteristic ionic spacing.

The *in situ* formation of the SG phase is therefore expected to interact with this pre-existing organization and act as a structural template for the ionic network.

Recently, E. Ferri *et al.* reported hybrid sPEEK membranes incorporating thiourea-functionalized SG phases, which act as sacrificial antioxidants.[64,65,82,83] By tailoring the chemistry, membranes containing up to 30 wt% SG showed improved thermomechanical stability. Tougne *et al.* further demonstrated, through *ex situ* ageing experiments and accelerated stress tests, that sPEEK membranes impregnated with 7 wt% of a SG phase derived from N,N'-bis[3-(triethoxysilyl)propyl] thiourea (HTU) or N-phenyl,N'-[3-(triethoxysilyl)propyl]thiourea (TTU) exhibited markedly enhanced durability under fuel cell operating conditions.[64,65] Both organosilane precursors contain a thiourea functional group, well known for its strong antioxidant properties.[84–86] The thiourea-functionalized SG phase preferentially reacts with oxidative species, providing total protection that fully suppresses degradation of the sPEEK matrix (no infrared absorption band at 1735cm^{-1} characteristic of the sPEEK oxidation) for up to 24 h at 80 °C in hydrogen peroxide concentrations as high as 0.15 % (≈ 40 mM). The progressive oxidation of the thiourea groups leads to their gradual consumption and to the formation of carbamic acid groups (increase of the absorption intensity at 1700 cm^{-1}). Beyond this threshold, the SG phase still provides

View Article Online
DOI: 10.1039/D6TA03128E

secondary protection, in which the oxidation rate is reduced compared to that of an unstabilized system, thereby significantly limiting membrane degradation.

In this work, we perform an in-depth analysis of thiourea-functionalized SG nanostructure using contrast-variation small-angle neutron scattering (CV-SANS), complemented by TEM and AFM. CV-SANS reveals that the SG phase is distributed both within ionic nanochannels and interbundle regions, with SG confined in the ionic domains playing a key protective role. By establishing this structure-property relationship, we provide new insights into how thiourea-based membranes confer oxidative protection.[64,65]

2. EXPERIMENTAL SECTION

2.1. Materials

The sPEEK host membrane was a Fumapem® E730 product from Fumatech (Germany), with a thickness of 30 µm and an ion exchange capacity (IEC) of 1.4 meq.g^{-1}. The hybridization process was previously reported by Ferri *et al.*.[82,83] HTU SG precursor (N, N'-bis[3-(triethoxysilyl)propyl] thiourea (**Fig.1**), CAS number: 69952-89-2) is commercially available from Gelest (USA). TTU SG precursor (N-phenyl,N'-[3-(triethoxysilyl)propyl]thiourea) was synthesized according to procedures reported by Ferri *et al.* (**Fig.1**).[82,83]

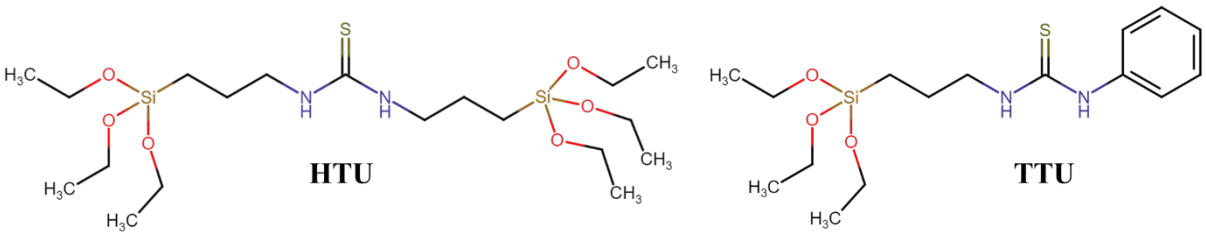

Fig. 1. Semi-developed structural formulas of the thiourea-based sol-gel precursors: N, N′-bis[3-(triethoxysilyl)propyl]thiourea (HTU) and N-phenyl,N′-[3-(triethoxysilyl)propyl]thiourea (TTU).[82,83]

2.2. Preparation of hybrid membranes

The preparation of hybrid membranes involved several sequential steps. First, sPEEK membranes were immersed in 1 M HCl at 30 °C for 4 h. This was followed by a hydrothermal treatment in liquid water at 80 °C for 72 h to improve the nanostructure.[81,87,88] Subsequently, a hydroalcoholic treatment in a 64/36 vol% water/ethanol mixture at room temperature and pH 4 was carried out for 24 h to swell the membrane in the solvent used for SG impregnation.

The SG precursors were pre-hydrolyzed separately at 0.1 mol. L^{-1} for 2 h at 30 °C in the same solvent mixture. The membranes were then immersed in this solution for 25 h at 30 °C, allowing the diffusion and *in-situ* growth of the reactive SG phase throughout the membrane core. Following impregnation, the membranes underwent a post-condensation step at 80 °C under nitrogen for 24 h to ensure complete condensation of the SG phase. A hydrothermal post-treatment (72 h in water at 80 °C) and a second

Open Access Article. Published on 11 June 2026. Downloaded on 6/12/2026 10:57:08 PM.
This article is licensed under a Creative Commons Attribution 3.0 Unported Licence.

Journal of Materials Chemistry A Accepted Manuscript

View Article Online
DOI: 10.1039/D6TA03128E

acidification step were subsequently applied to remove uncondensed SG oligomers and restore all sulfonic groups to their acidic form. Hybrid membranes with varying SG loadings (10-30 wt%) were prepared to investigate the effect of SG chemistry and uptake on membrane morphology and functional properties. Morphological characteristics were compared with a reference sPEEK membrane (referred to as "pristine") that underwent identical treatments but without SG precursors.[82,83]

2.3 Gravimetric measurements

(i) Water uptake

The water uptake (WU_{pt}) of the membranes was determined at room temperature after a 72 h swelling period in liquid water at 80 °C, followed by equilibration back to room temperature. Prior to weighing, any excess surface water was carefully removed using absorbent paper. The water uptake was calculated according to Equation (1):

$$WU_{pt} = \frac{mHyb_{wet} - mHyb_{dry}}{mHyb_{dry}} \times 100\ \% \quad (1)$$

where, $mHyb_{dry}$ and $mHyb_{wet}$ correspond to the masses of the hybrid membrane in the dry and wet states, respectively. The dry mass $mHyb_{dry}$was measured after drying the membrane under a nitrogen flow at room temperature for at least 24 h.

(ii) Density

The density of the membranes was determined using a helium pycnometer (AccuPyc II 1340, Micromeritics®). The sample volume was measured from pressure variations according to Mariotte's law. Prior to measurement, all samples were thoroughly dried overnight under a nitrogen flow at room temperature to ensure complete removal of moisture.

2.4 Proton conductivity

The in-plane proton conductivity of the membranes was measured at room temperature using a four-electrodes configuration.[89] Measurements were performed by linear sweep voltammetry using an Essential VSP potentiostat (BioLogic Science Instrument) coupled to a BT-110 conductivity cell (Scribner Inc., USA). Prior to measurement, the membranes were immersed in deionized water at 80 °C for 72 h, then re-acidified in 1 M HCl at room temperature for 4 h, and finally rinsed three times with deionized water. The in-plane resistance (R, Ω) was determined from the current–voltage curve. The proton conductivity (σ, $S.cm^{-1}$) was then calculated using Equation (2):

$$\sigma = \frac{L}{W \times e \times R} \quad (2)$$

Open Access Article. Published on 11 June 2026. Downloaded on 6/12/2026 10:57:08 PM.
This article is licensed under a Creative Commons Attribution 3.0 Unported Licence.

Journal of Materials Chemistry A Accepted Manuscript

View Article Online
DOI: 10.1039/D6TA03128E

where L is the distance between the electrodes (cm), W is the membrane width (cm), and e is the membrane thickness (cm).

2.5 Aging protocol

The aging of the membranes was performed *ex situ* using the hydrogen peroxide degradation method described by Tougne *et al.*.[64,65] Chemical degradation was thermally activated by immersing the membranes at 80 °C for 24 h in aqueous H_2O_2 solutions of varying concentrations, ranging from 0.025 to 1 wt% (7.4 to 294 mM). Each membrane sample was immersed in a fixed solution volume (2 mL per mg of dry membrane) to ensure consistent exposure conditions. During the aging experiments, the membranes were kept fully submerged in the H_2O_2 solution using an inert glass rod to prevent floating throughout the exposure period.

2.6 Morphological analysis by Small-Angle Neutron Scattering (SANS)

SANS measurements were performed on the D22 beamline at the Institut Laue-Langevin (ILL, Grenoble, France) using a neutron wavelength $\lambda = 6$ Å. The scattering vector q is defined as in Equation (3):

$$q = \frac{4\pi}{\lambda}\sin\theta \tag{3}$$

where 2θ is the total scattering angle.

Membranes were swollen in water at 80 °C for 72 h and equilibrated in H_2O, D_2O, or H_2O/D_2O mixtures for at least 24 h. Hydrated stacks of 3-5 membranes were mounted in 1 mm quartz holders sealed with O-rings. Measurements were performed at two sample-to-detector distances (2.8 m and 17.6 m), covering a scattering vector range of $2.5\times10^{-3} < q < 0.4$ Å^{-1} (~15–2500 Å). Spectra were corrected for detector efficiency, background scattering, and empty-cell contributions, and absolute intensities were obtained using the direct beam.

For biphasic systems, the scattered intensity provides information on particle shape (form factor P(Q)), and spatial organization (structure factor S(Q)). For N□ centrosymmetric particles of volume V□, the scattering intensity per unit sample volume V can be expressed as Equation (4):

$$I(q) = \frac{{V_p}^2}{V} N_p.{\Delta\rho}^2.P(q).S(q) = \Phi.V_p.{\Delta\rho}^2.P(q).S(q) \tag{4}$$

where Φ is the particle volume fraction and $(\Delta\rho)^2$ is the squared difference in scattering length density (SLD) between particle and medium.

Open Access Article. Published on 11 June 2026. Downloaded on 6/12/2026 10:57:08 PM.
This article is licensed under a Creative Commons Attribution 3.0 Unported Licence.

Journal of Materials Chemistry A Accepted Manuscript

View Article Online
DOI: 10.1039/D6TA03128E

For triphasic systems, such as hybrid membranes composed of sPEEK, sol-gel, and the surrounding medium, the total scattering intensity combines contributions from sPEEK (number of atoms in the repeating unit sPEEK), sol-gel ($I(Q)_{SG}$), and a cross-term ($I(Q)_{cross}$) as given in Equation (5):

$$I(q)_{total} \propto (\Delta\rho_{sPEEK})^2 I(q)_{sPEEK} + (\Delta\rho_{SG})^2 I(q)_{SG} + \Delta\rho_{sPEEK}\Delta\rho_{SG} I(q)_{cross} \quad (5)$$

Contrast variation SANS (CV-SANS) was employed to selectively probe each phase. By systematically adjusting the solvent SLD of using H_2O/D_2O mixtures, the contrast of one phase can be matched ($\Delta\rho = 0$). According to Eq. (5), this suppresses both its self-correlation term $(\Delta_\rho)^2 I(q)$ and the cross-term contribution $\Delta\rho_{sPEEK}\Delta\rho_{SG} I(q)_{cross}$. The remaining intensity thus originates predominantly from the unmatched phase.

In the present hybrid membranes, the SG phase could not be measured independently, as its structure and density in *ex situ* form differ from those formed *in situ* within the membrane. Determination of the true *in situ* SG contrast matching point would require selective removal of the sPEEK host matrix, which is destructive and may alter the SG nanostructure. Nevertheless, the SG contrast matching point was estimated from its chemical composition and bulk density, and subsequently validated experimentally. This validation is possible because the SG scattering dominates at low q values, allowing a reliable determination of the matching condition (see **Fig. S1** and **S2**).

It should be recalled that the scattering length density (SLD) of a phase is given by Equation (6):

$$\text{SLD} = \rho = \frac{\sum_i x_i b_i}{V_p} = \frac{\sum_i b_i d N_a}{M} \quad (6)$$

where b_i are the atomic scattering length, x_i the number of atoms in the repeating unit, V_p is the particle volume, d the phase density, N_a is Avogadro's number, and M is the molar mass.

Therefore, the experimentally determined SLD (e.g., obtained by contrast variation SANS) can be used to calculate the corresponding density of the solid phase (see **Table 1** for the SLD, contrast $\Delta\rho^2$, and D_2O fraction corresponding to the contrast matching of sPEEK, SG HTU, and SG TTU phases).

Table 1. Scattering length density (SLD), contrast $\Delta\rho^2$, and D_2O fraction corresponding to the contrast matching of sPEEK, SG HTU, and SG TTU phases.

SLD	Phase	sPEEK	SG HTU	SG TTU	56%D_2O (sPEEK match)	18%D_2O (SG HTU match)	25%D_2O (SG TTU match)	100%D_2O
	ρ (10^{10} cm^{-2})	3.34	1.26	1.74	3.33	0.69	1.18	6.39
$\Delta\rho^2$	sPEEK		4.33	2.56	≈ 0	7.02	4.67	9.30
	SG HTU	4.33			4.29	≈ 0		26.30

Open Access Article. Published on 11 June 2026. Downloaded on 6/12/2026 10:57:08 PM.
This article is licensed under a Creative Commons Attribution 3.0 Unported Licence.

Journal of Materials Chemistry A Accepted Manuscript

View Article Online
DOI: 10.1039/D6TA03128E

SG TTU	2.56		2.53		≈ 0	21.60

2.7 Morphological imaging by AFM and TEM

(i) Sample preparation by cryo-ultramicrotomy

Samples of hybrid membranes with a thickness of approximately 30 µm were trimmed and sectioned using a LEICA EM UC7 cryo-ultramicrotome at -120 °C in order to produce a flat surface of about 200 × 30 µm^2. Membranes were cut without epoxy embedding and secured in a vice, thus avoiding any potential chemical contamination. The sample surface was required to protrude no more than about 50 µm above the vice top surface (to prevent membrane flexion during AFM analysis). The surface of the cryo-ultramicrotomy cross-sectioned provides a sample suitable for AFM analysis. At the same time, ultrathin sections (~100 nm thick) were collected for complementary analysis by Transmission Electron Microscopy (TEM).

(ii) AFM

Topographic and mechanical images of the hybrid membranes were obtained using PeakForce QNM mode on a Nanoscope Dimension ICON AFM (Bruker). All measurements were performed under ambient conditions with a standard cantilever holder for operation in air. Relative calibration was carried out using a dedicated reference sample kit provided by Bruker (Model: PFQNM-SMPKIT-12M); more details about the calibration process are provide by Cosas Fernandes *et al.*[90] The HTU hybrid membranes were analyzed by AFM using two types of tips: ScanAsyst (flexible cantilever with stiffness k = 0.4 N/m, radius of curvature d ~5 nm) for shallow penetration into the sample and high-quality topographic imaging, and OTESPA-R3 (stiffer cantilever with stiffness k = 26 N/m, larger radius of curvature d = 7–10 nm) for deeper penetration and high-quality mechanical imaging (at the expense of topographic resolution).

(iii) TEM

Thin sections of membranes (~100 nm thick) were collected by cryo-ultramicrotomy on carbon lacey covered copper grids. They were analyzed using a Tecnai F20 field emission gun (FEG) TEM (FEI) at an accelerating voltage of 200 kV, without any staining, with contrast between the sPEEK and SG phases being expected.

3. RESULTS AND DISCUSSION

3.1 Nanostructure of sPEEK phase in hybrid membranes and structure-property interplay

To assess the impact of the SG phase on the nanostructure of the sPEEK matrix, CV-SANS measurements were performed under conditions where the SG scattering was selectively matched out. The D_2O fraction required for contrast matching was first estimated from the SG chemical composition

Open Access Article. Published on 11 June 2026. Downloaded on 6/12/2026 10:57:08 PM.
This article is licensed under a Creative Commons Attribution 3.0 Unported Licence.

Journal of Materials Chemistry A Accepted Manuscript

View Article Online
DOI: 10.1039/D6TA03128E

and bulk density (Experimental Section, § 2.5). Although the SG phase cannot be measured independently (Experimental Section, § 2.5), the matching point could be validated experimentally, as SG scattering dominates at low q values, allowing reliable determination by varying the H_2O/D_2O ratio until the SG contribution was minimized. Extinction of the SG signal was achieved at 18 % D_2O for the HTU membrane, whereas only partial suppression was obtained at 25 % D_2O for the TTU membrane. In both cases, the sPEEK ionomer peak remained clearly detectable, showing that the nanostructure is preserved upon hybridization, and enabling independent analysis of the ionic domains relative to the SG phase (**Fig. S1**).

The SANS profiles of HTU and TTU hybrid membranes (**Fig. 2a** and **2c**) show discernible ionomer peaks, allowing determination of the ionic channel spacing d_{iono} using Bragg's law (**Eq. 7**).

$$d_{iono} = \frac{2\pi}{q_{iono}} \quad (7)$$

These structural parameters were subsequently correlated with water uptake and proton conductivity, highlighting the link between nanoscale organization and macroscopic properties (**Fig. 2b** and **2d**).

HTU membranes containing 7.5, 14, and 24 wt% SG (**Fig. 2a**) exhibit a pronounced shift of the ionomer peak from q = 0.085 $Å^{-1}$ in pristine sPEEK (100 % D_2O) to q = 0.15 $Å^{-1}$ at 24 wt% SG, corresponding to a decrease in the ionic channel spacing d_{iono} from 87 Å to 45 Å. Concurrently, water uptake decreases from 203 to 39 %, and proton conductivity drops from 70 to 7 $mS.cm^{-1}$, indicating that increasing HTU content constrains swelling of the ionic domains, reducing their effective size and strongly affecting transport properties, while the overall nanostructure of the membrane is preserved (**Fig. 2b**).

In contrast, TTU membranes containing 9 and 20 wt% SG (**Fig. 2c**) show a more gradual shift of the ionomer peak q_{iono} from 0.085 to 0.089 $Å^{-1}$, corresponding to a reduction of d_{iono} from 74 to 71 Å. The associated decreases in water uptake (from 203 to 143 %) and proton conductivity (from 70 to 53 $mS.cm^{-1}$) indicate that the TTU SG phase impacts the ionomer nanostructure and functional properties to a lesser extent than HTU (**Fig.2b**).

Overall, increasing SG content - corresponding to a decrease in the sPEEK volume fraction - leads to a decrease in both water uptake and proton conductivity, in agreement with previous reports.[83] Proton conductivity remains at a level compatible with fuel cell operation (~50 $mS.cm^{-1}$) up to about 7-10 wt% SG. The more pronounced decrease observed for HTU membranes can be attributed to the hexafunctional character of the HTU siloxane fragments, which promotes the formation of a more highly connected SG network. This increased crosslinking strongly constrains swelling of the ionic domains, thereby reducing water uptake and proton transport.

As shown in **Fig. 2b** and **2d**, when water uptake is considered relative to the sPEEK volume fraction (upper axis), the amount of sorbed water associated with the polymer phase decreases more markedly in HTU membranes than in TTU ones. This trend indicates that the reduction in water uptake and proton

Open Access Article. Published on 11 June 2026. Downloaded on 6/12/2026 10:57:08 PM.
This article is licensed under a Creative Commons Attribution 3.0 Unported Licence.

Journal of Materials Chemistry A Accepted Manuscript

View Article Online
DOI: 10.1039/D6TA03128E

conductivity beyond 10 wt% SG is primarily due to constrained swelling of the ionic domains by the SG network, rather than a simple dilution of the polymer. While TTU membranes also show some decrease in hydration and transport at higher SG contents, these effects are less pronounced than in HTU membranes.[83]

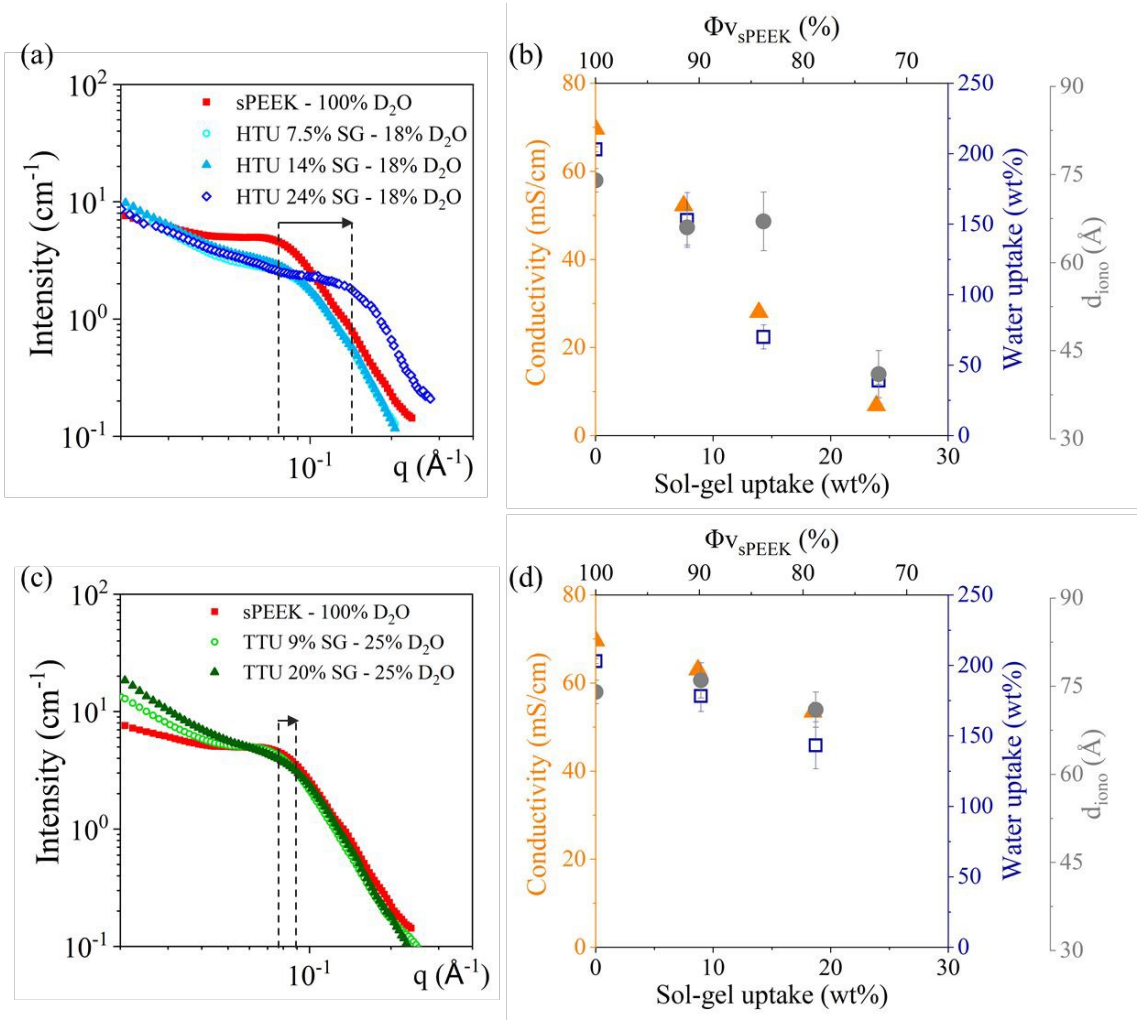

Fig. 2. (a, c) SANS profiles of the sPEEK membrane measured in 100 % D_2O (■) and hybrid membranes containing HTU-based SG at 7.5, 14 and 24 wt% SG (○, ▲ ,◇) measured in 18 % D_2O, and TTU-based SG at 9 and 20 wt% (○, ▲) measured in 25% D_2O. (b, d) Proton conductivity, water uptake and ionic channels spacing of HTU- and TTU-based hybrid membranes, respectively, plotted as a function of SG uptake and sPEEK volume fraction (Φ_v).

3.2. Multiscale morphology of SG phase in HTU and TTU hybrid membranes

The distribution and mesostructure of the SG phase in hybrid membranes were investigated by SANS under hydrated conditions with 56 % D_2O (matching the sPEEK signal; see **Fig. S2**) as well as in dry state. These SANS measurements were complemented by TEM and AFM analyses to further characterize the membrane morphology across different length scales.

(i) SANS analysis

Open Access Article. Published on 11 June 2026. Downloaded on 6/12/2026 10:57:08 PM.
This article is licensed under a Creative Commons Attribution 3.0 Unported Licence.

Journal of Materials Chemistry A Accepted Manuscript

View Article Online
DOI: 10.1039/D6TA03128E

HTU membranes. In the hydrated state, a broad scattering feature is observed at q ≈ 0.078 Å^{-1}, in the same angular range as the ionomer peak of pristine sPEEK (**Fig. 3a**). In this work, this contribution is referred to as the *hybrid peak*. Its coincidence in q-position with the pristine ionomer peak, and its clear intensity under SG contrast-matching conditions, indicate that SG domains are confined within, or strongly associated with, the sPEEK ionic channel network formed during SG synthesis.

Importantly, the persistence of the ionomer peak under SG contrast-matching conditions (**Fig. 2a**) indicates that the ionic channels remain accessible to solvent, with the SG phase partially occupying the domains and constraining their swelling while still allowing hydration of the ion channel network.

The large width of the hybrid feature indicates that SG incorporation is spatially heterogeneous at the nanoscale. This results in a distribution of local spacings rather than a well-defined periodic structure. The intensity of the hybrid peak increases slightly with SG loading (7.5-14 wt%), while its position remains essentially unchanged, indicating preservation of the characteristic correlation length of the ionic domains.

A similar scattering feature has been reported for sol-gel-derived Nafion-SiO_2 systems where it was attributed to silica growth within ionic channels during processing, supporting the notion of nanoscale confinement in hybrid ionomer systems.[91]

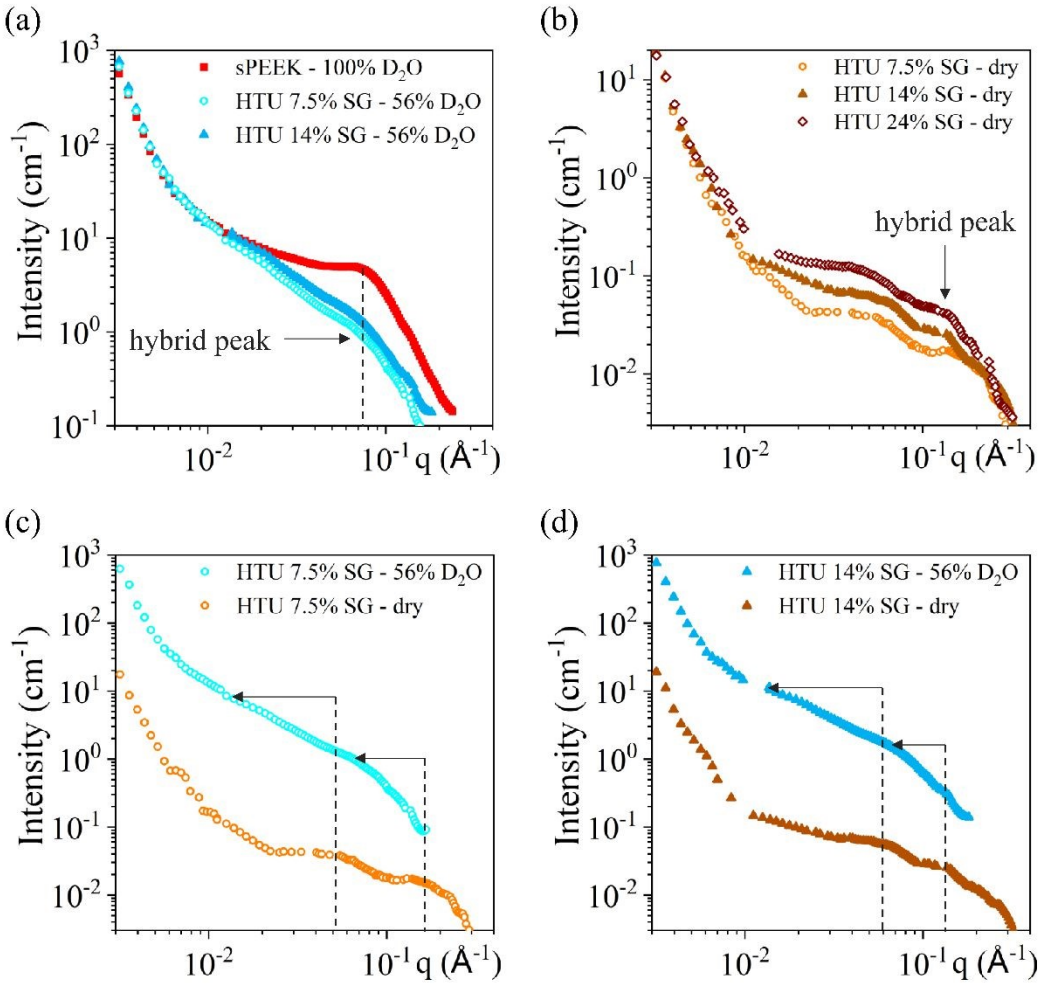

Open Access Article. Published on 11 June 2026. Downloaded on 6/12/2026 10:57:08 PM.
This article is licensed under a Creative Commons Attribution 3.0 Unported Licence.

Journal of Materials Chemistry A Accepted Manuscript

View Article Online
DOI: 10.1039/D6TA03128E

Fig. 3. SANS profiles of (a) the sPEEK membrane in 100 % D_2O (■) and hybrid membranes HTU 7.5 and 14 wt% SG (○, ▲) in 56 % D_2O. (b) HTU hybrid membranes containing 7.5, 14 and 24 wt% SG (○, ▲, ◇) measured in dry state. Comparison between wet and dry state of (c) HTU 7.5 wt% and (d) HTU 14 wt%.

Dry conditions are particularly informative (**Fig. 3b**). Indeed, in the dry state, pristine sPEEK shows no detectable ionomer peak, as the scattering contrast between the sPEEK matrix and the ionic domains vanishes (**Fig. S2c**).[81] In dry hybrid membranes, scattering is dominated by the SG phase via SG/sPEEK contrast. The hybrid peak shifts toward lower q values between 7.5 and 14 wt% SG and then evolves only slightly up to 24 wt%, corresponding overall to an increase in the characteristic spacing from 36 to 44 Å. This behavior suggests that SG incorporation within the ionic domains of the membrane mainly occurs between 7.5 and 14 wt% SG, while higher SG loadings primarily increase the amount of SG located in interbundle regions without significantly modifying the characteristic nanoscale spacing. The increase in scattering intensity with SG loading is likely associated with the larger amount of HTU-derived SG phase present in the interbundle regions, together with a progressive rigidification -and thus densification -of the formed SG network, HTU being a hexafunctional precursor.

The hybrid peak positions and corresponding Bragg spacings for HTU membranes containing 7.5, 14 and 24 wt% SG, are summarized in **Table 2**.

Table 2. Hybrid peak positions and corresponding Bragg spacings for HTU hybrid membranes containing 7.5, 14 and 24 wt% SG.

HTU hybrid membrane	7.5 wt% SG		14 wt% SG		24 wt% SG
	Dry	Hydrated	Dry	Hydrated	Dry
q_{hybrid} (Å^{-1})	0.18 ± 0.01	0.077 ± 0.008	0.14 ± 0.01	0.079 ± 0.004	0.14 ± 0.01
d_{hybrid} (Å)	36 ± 3	82 ± 8	44 ± 2	80 ± 4	44 ± 2

At smaller angles (q = 0.02-0.09 Å^{-1}, **Fig. 3b**), a broad feature indicates the presence of relatively large sPEEK/SG domains, likely located in interbundle regions.[92] Guinier analysis of this low-q region yields radii of gyration Rg ≈ 1.8-2.3 nm[93] (**Fig. S3 a, b; Table S3 a**), corresponding to geometric radii of approximately 2.3-2.9 nm (diameters ~5-6 nm), assuming spherical domains (Rg^2=3/5 Rg^2). This spherical model is consistent with the nearly constant intensity at very low q and the q^{-4} decay at higher q, and is further confirmed by fitting the low-q region with a spherical form factor using SASView (**Fig. S3c, Table S3b**).

In hydrated membranes (**Fig. 3c, d**), this feature shifts slightly toward lower q, reflecting an increase in spacing between interbundle domains. The size and shape of these domains, however, remain essentially unchanged with increasing SG uptake, indicating no significant evolution of the morphology of these

Open Access Article. Published on 11 June 2026. Downloaded on 6/12/2026 10:57:08 PM.
This article is licensed under a Creative Commons Attribution 3.0 Unported Licence.

Journal of Materials Chemistry A Accepted Manuscript

View Article Online
DOI: 10.1039/D6TA03128E

SG domains upon hydration. Consequently, increasing SG loading primarily increases the number of SG-containing interbundle domains, rather than the size of individual domains (**Fig. 3b**).

To further support the validity of this structural description, a comparison between SANS and SAXS profiles measured simultaneously under hydrated conditions (100% D_2O) on the D22 instrument at the ILL are shown in **Fig. S3**. Both techniques exhibit consistent scattering features, supporting the presence of the same characteristic nanoscale organization and reinforcing the robustness of the proposed interpretation.

TTU membranes. TTU hybrid membranes exhibit SANS features similar to HTU membranes, but with a distinct SG organization. In hydrated TTU membranes (9-20 wt% SG) under sPEEK-matched conditions, the hybrid peak remains centered at $q \approx 0.084$ Å^{-1}, indicating uniform filling of the ionic channels, essentially independent of SG content (**Fig. 4a**). Its intensity increases slightly with increasing SG loading, suggesting a limited increase in the amount of SG confined within the ionic domains. In dry membranes, the hybrid peak shifts to higher q values (≈ 0.16 Å^{-1}) and becomes broader, reflecting a wider distribution of characteristic spacings between SG domains within the ionic channels and a more heterogeneous SG organization compared to HTU (**Fig. 4b**).

Open Access Article. Published on 11 June 2026. Downloaded on 6/12/2026 10:57:08 PM.
This article is licensed under a Creative Commons Attribution 3.0 Unported Licence.

Journal of Materials Chemistry A Accepted Manuscript

View Article Online
DOI: 10.1039/D6TA03128E

Open Access Article. Published on 11 June 2026. Downloaded on 6/12/2026 10:57:08 PM.
This article is licensed under a Creative Commons Attribution 3.0 Unported Licence.

Journal of Materials Chemistry A Accepted Manuscript

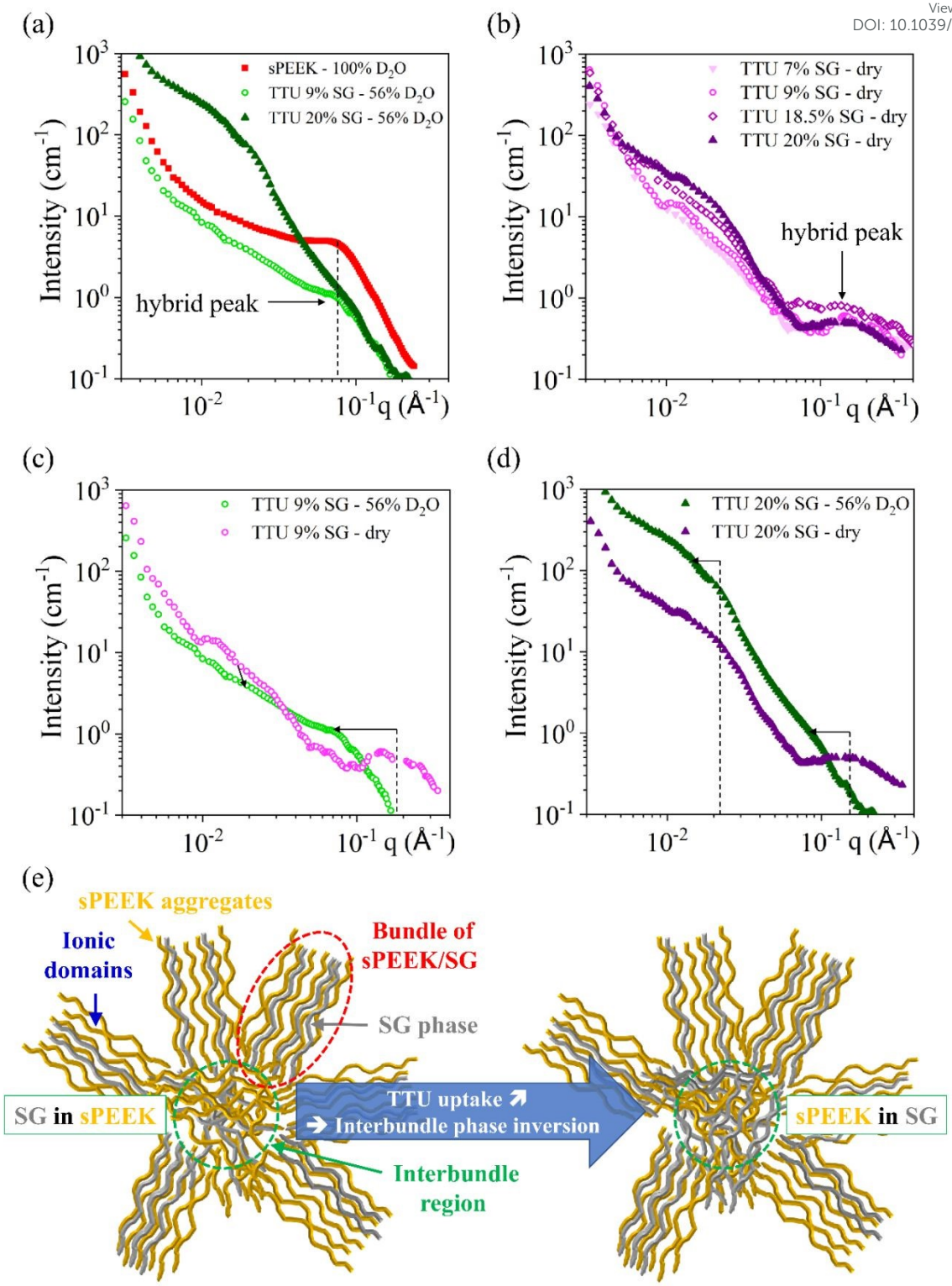

Fig. 4. SANS profiles of (a) the sPEEK membrane in 100 % D_2O (■) and TTU hybrid membranes containing 9 and 20 wt% SG (○, ▲) measured in 56% D_2O. (b) Dry-state SANS profiles of TTU hybrid membranes containing 7, 9, 18.5, and 20 wt% SG (▼, ○, ◇, ▲). Comparison between hydrated and dry state for (c) TTU 9 wt% and (d) TTU 20 wt% hybrid membranes (e) Schematic illustration of the phase inversion in interbundle regions with increasing uptake: SG-in-sPEEK → sPEEK-in-SG.

View Article Online
DOI: 10.1039/D6TA03128E

At smaller angles (q = 0.005-0.08 Å^{-1}, **Fig. 4b)**, a broad feature corresponds to interbundle SG/sPEEK domains, with radii of gyration Rg ≈ 9-11 nm (domain diameters ~18-22 nm; **Fig. S5, Table S5**). While domain size remains essentially constant, increased SG content raises scattering intensity, indicating a higher number of interbundle domains rather than growth of individual domains.

Upon hydration, the interbundle signal shifts slightly toward lower q, reflecting increased spacing between domains (**Fig. 4c, d**). The evolution of scattering intensity depends strongly on SG content. In low-SG membranes (9 wt%), intensity decreases upon swelling. Because $I(q) \propto NV^2S(q)P(q)\Delta\rho^2$, and the contrast term ($\Delta\rho^2$) remains unchanged between the dry and hydrated states due to sPEEK contrast matching in 56% D_2O, this decrease reflects a reduction of the effective scattering volume V rather than contrast effects, consistent with compression of the SG-rich interbundle regions by the expanding sPEEK matrix. In high-SG membranes (20 wt%), intensity increases, indicating expansion of SG-rich domains. These opposite trends indicate a phase inversion in the interbundle region: at low SG content, SG domains are dispersed within a continuous sPEEK matrix, whereas at high SG loading, the sPEEK domains become embedded in a continuous SG-rich phase. Beyond a certain SG content, additional SG no longer enters the ionic channels but localizes in the interdomain regions of the bundles, consistent with the observation that the high-q peak remains largely unchanged. A schematic representation illustrating this phase inversion mechanism is provided in **Fig. 4e**.

The hybrid peak positions and corresponding Bragg spacings for TTU membranes containing 9 and 20 wt% SG, are summarized in **Table 3**.

Table 3. Hybrid peak positions and corresponding Bragg spacings for TTU hybrid membranes containing 9 % and 20 wt% SG.

TTU hybrid membrane	9 wt% SG		20 wt% SG	
	Dry	Hydrated	Dry	Hydrated
q_{hybrid} (Å^{-1})	0.17 ± 0.01	0.079 ± 0.004	0.15 ± 0.01	0.091 ± 0.004
d_{hybrid} (Å)	38 ± 2	80 ± 4	41 ± 2	69 ± 3

(ii) Microscopy observations

TEM images of ultrathin cross-sections of sPEEK, HTU 18 %, and TTU 18 % hybrid membranes are shown in **Fig. 5.**

Open Access Article. Published on 11 June 2026. Downloaded on 6/12/2026 10:57:08 PM.
This article is licensed under a Creative Commons Attribution 3.0 Unported Licence.

Journal of Materials Chemistry A Accepted Manuscript

View Article Online
DOI: 10.1039/D6TA03128E

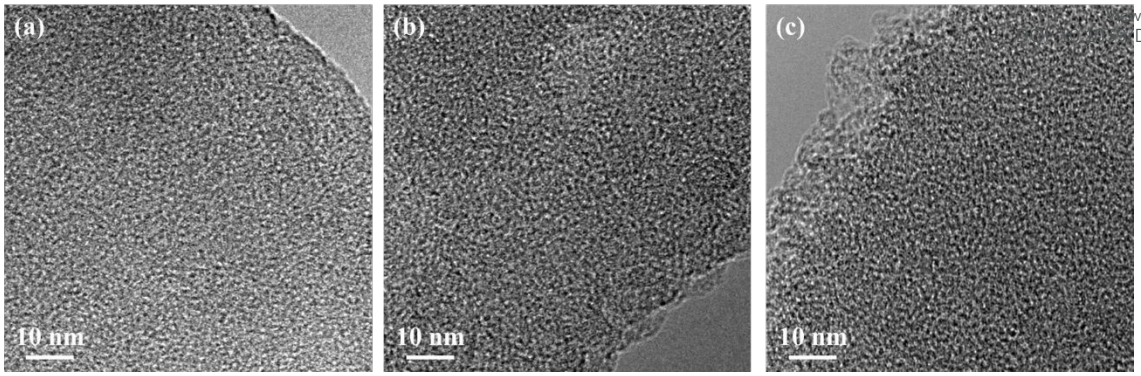

Fig. 5. TEM images of ultrathin cross-sections of membranes: (a) pristine sPEEK, (b) HTU hybrid with 18 wt% SG, and (c) TTU hybrid with 18 wt% SG.

TEM images show that both pristine sPEEK and the hybrid membranes appear homogeneous with similar amorphous contrast. No distinct SG domains are observed in either HTU or TTU membranes. In particular, features corresponding to the expected SG domain sizes (~5-6 nm for HTU and ~14 nm for TTU) are not resolved, indicating that the SG phase is either uniformly dispersed at the nanoscale or that the electron density contrast between SG and sPEEK is too low to distinguish individual domains. In a similar manner, AFM modulus images (**Fig. 6**) reveal no detectable morphological changes upon SG incorporation, and no SG-rich domains are observed, contrary to previous results reported for hybrids prepared with (3-mercaptopropyl)trimethoxysilane precursors.[63] Therefore, both AFM and TEM observations indicate that dry HTU and TTU membranes exhibit no discernible contrast between the sPEEK and SG phases, confirming intimate nanoscale mixing. The absence of sharply segregated domains supports the interpretation that the SANS signal arises from nanoscale density fluctuations associated with the SG phase distributed within both the ionic domains and the interbundle regions, rather than from discrete, phase-separated SG particles.

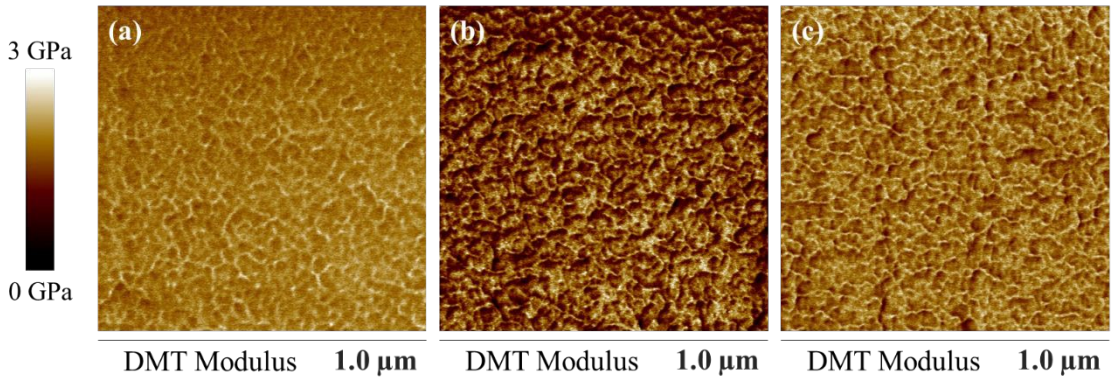

Fig. 6. AFM modulus images of opened cross-sections of membranes: (a) pristine sPEEK, (b) HTU hybrid containing 7 wt% SG, and (c) TTU hybrid containing 18 wt% SG.

(iii) Morphological scenario

Open Access Article. Published on 11 June 2026. Downloaded on 6/12/2026 10:57:08 PM.
This article is licensed under a Creative Commons Attribution 3.0 Unported Licence.

Journal of Materials Chemistry A Accepted Manuscript

View Article Online
DOI: 10.1039/D6TA03128E

The absence of discernible domains in TEM and AFM indicates that the SANS signal arises from nanoscale density fluctuations rather than from discrete SG particles. Two main SANS contributions are identified: (i) a *hybrid peak*, associated with SG confined within the ionic nanochannels, and (ii) a small-angle contribution originating from the inhomogeneous distribution of SG within the ionic domains and interbundle regions, generating local density contrasts.

In HTU membranes, the fraction of SG confined within the channels increases at low SG contents (up to ~14 wt%), before reaching a regime where additional SG does not significantly contribute to further channel filling and is preferentially located in interbundle regions. The resulting decrease in proton conductivity and hydration is primarily attributed to the hexafunctional and strongly crosslinked nature of the SG network, which limits proton transport pathways. The number of ~5 nm sPEEK/SG interbundle domains increases with SG content, while their characteristic size remains essentially unchanged, indicating an increased population of such domains (see **Fig. S4c**, **Table S4b**).

In TTU membranes, SG are confined, but its proportion remains essentially constant with increasing SG content, likely due to the lower connectivity of the trifunctional TTU network compared to the hexafunctional HTU (~14 nm) become more numerous and exhibit opposite responses to hydration depending on SG loading: they contract at low SG content (9 wt%) and expand at high SG content (20 wt%). This behavior is consistent with a phase-inversion mechanism in the interbundle region, where SG phase is dispersed within a continuous sPEEK matrix at low SG content, whereas at higher loading, sPEEK domains are embedded within a SG-rich continuous phase. Although phase inversion often affects functional properties, here the transition occurs mainly in the interbundle regions rather than in the ionic channels that govern hydration and proton transport. In the pristine state, its direct impact on transport is limited; however, the interbundle regions act as bridges between ionic domains, maintaining structural cohesion and potentially modulating the accessibility and consumption of SG under oxidative stress. Overall, these results reveal an interpenetrated sPEEK/SG network, in which nanoscale density fluctuations influence both the ionic channels and the interbundle regions.

To establish a direct link between nanoscale organization and chemical durability, the following section examines the structural evolution of the hybrid membranes under oxidative stress. By combining accelerated aging in H_2O_2 with SANS measurements, we investigate how exposure to increasing oxidant concentration affects the morphology and accessibility of the SG phase, and how these changes correlate with the loss of proton conductivity and mechanical integrity.

3.3 Chemical-degradation-induced morphological evolution of sPEEK and SG phases

The location and accessibility of thiourea functions within the SG phase play a key role in the protection of the sPEEK matrix. *Ex situ* accelerated aging experiments showed that hybrid membranes remain fully protected up to 0.15 wt% H_2O_2, while degradation proceeds at a significantly reduced rate compared to pristine sPEEK at higher oxidant concentrations.[65] These results highlight the critical role of thiourea-based hybridization in mitigating oxidative degradation. To elucidate the structural origins of this

Open Access Article. Published on 11 June 2026. Downloaded on 6/12/2026 10:57:08 PM.
This article is licensed under a Creative Commons Attribution 3.0 Unported Licence.

Journal of Materials Chemistry A Accepted Manuscript

View Article Online
DOI: 10.1039/D6TA03128E

enhanced durability, we investigate how the morphologies of both the sPEEK matrix and the SG phase evolve under increasing oxidative stress. Contrast-variation SANS is used to monitor changes in the spatial distribution and accessibility of the SG phase as the system shifts from total oxidative protection to a regime of slowed degradation.

(i) Nanostructure of the sPEEK phase in pristine vs hybrid membranes

Fig. 7a shows the evolution of the SANS profile of a sPEEK membrane as a function of H_2O_2 concentration. The associated structural changes, evidenced by the shift in d_{iono}, directly correlate with variations in water uptake and proton conductivity (**Fig. 7b**).

With increasing H_2O_2 concentration, the ionomer peak shifts to lower q values (from 0.090 to 0.055 $Å^{-1}$) up to 0.3 % H_2O_2, reflecting a pronounced expansion of the ionic domains (d_{iono} increasing from 70 to 115 Å). Water uptake rises similarly, from 165 % to 215 % up to 0.1 % H_2O_2. Above this concentration, the ionomer peak markedly broadens and becomes barely detectable, indicating extensive dilution of the polymer aggregates and loss of membrane cohesion, which prevents reliable measurement of water uptake. Radical-induced chain scission in the polymer reduces mechanical integrity and enhances swelling.[94] As the membrane absorbs water, small fragments, mainly cleaved sulfonated chains, are released from the backbone[65], explaining the concurrent drop in proton conductivity from 79 to 54 $mS.cm^{-1}$.

Open Access Article. Published on 11 June 2026. Downloaded on 6/12/2026 10:57:08 PM.
This article is licensed under a Creative Commons Attribution 3.0 Unported Licence.

Journal of Materials Chemistry A Accepted Manuscript

View Article Online
DOI: 10.1039/D6TA03128E

Open Access Article. Published on 11 June 2026. Downloaded on 6/12/2026 10:57:08 PM.
This article is licensed under a Creative Commons Attribution 3.0 Unported Licence.

Journal of Materials Chemistry A Accepted Manuscript

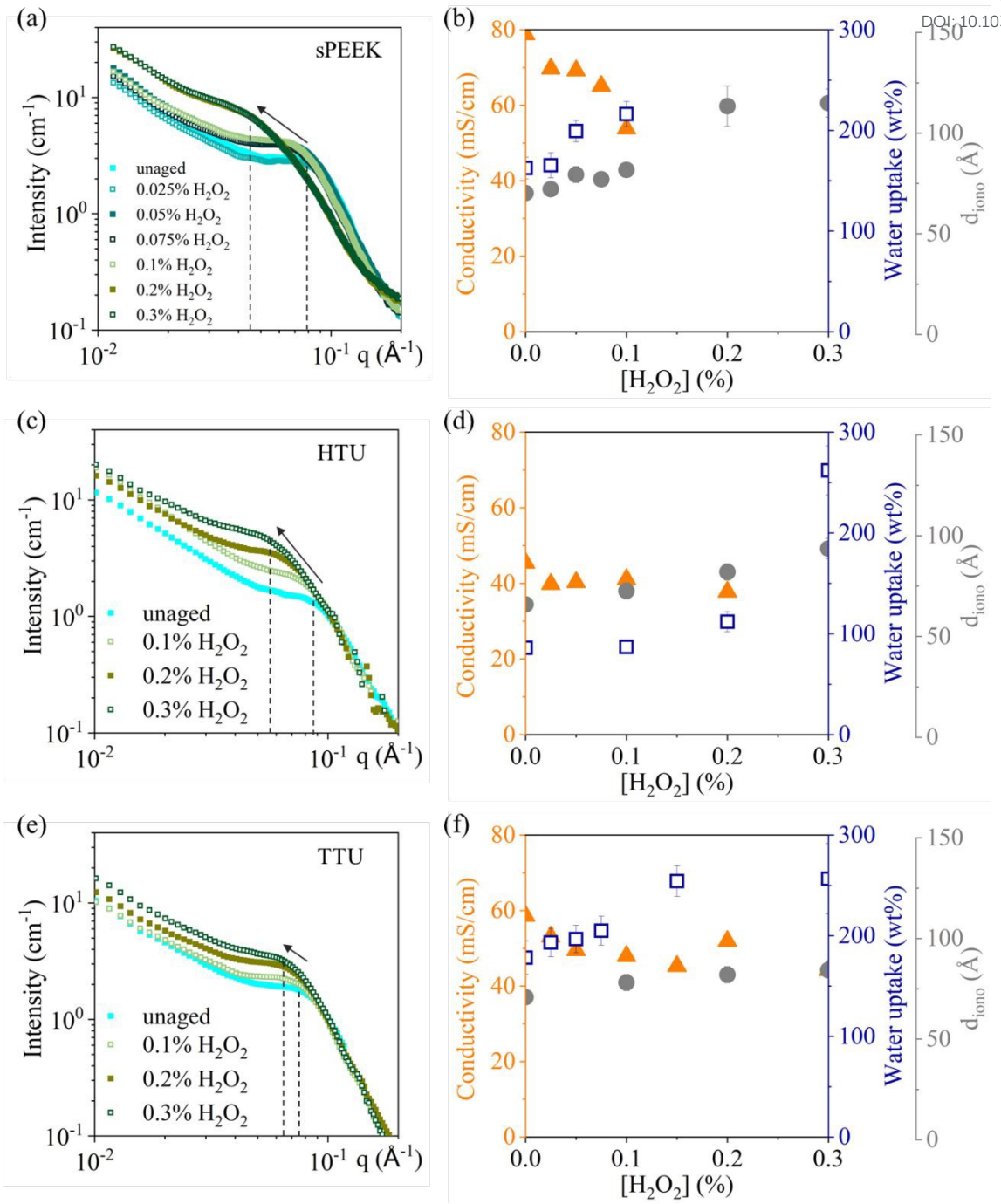

Fig. 7. (a) SANS profiles of sPEEK membranes aged for 24 h at 80 °C in H_2O_2 solutions (0.025–0.3%), followed by drying and re-swelling in H_2O prior to measurement. (b) Corresponding evolution of proton conductivity, water uptake, and ionic channel spacing (d_{iono}) of sPEEK as a function of H_2O_2 concentration. SANS profiles of (c) HTU and (d) TTU hybrid membranes aged in H_2O_2 solutions (0.1–0.3%) under the same protocol, then dried and rehydrated in H_2O/D_2O mixtures (18% D_2O for HTU, 25% D_2O for TTU). (e, f) Corresponding conductivity, water uptake, and ionic channel spacing (d_{iono}) of HTU and TTU membranes, respectively, as a function of SG content and sPEEK volume fraction.

This raises a key question for hybrid membranes: how does the nanoscale morphology and localization of the thiourea-based SG phase control the protection of the sPEEK matrix?

View Article Online
DOI: 10.1039/D6TA03128E

To address this question, the structural evolution of the sPEEK phase during aging was monitored by CV-SANS, using the initial D_2O concentrations that provide optimal contrast (18 % for HTU and 25 % for TTU membranes; see Section **2.5**). Although aging may induce minor changes in phase density, the contrast conditions remain sufficient to resolve the main structural features, enabling direct comparison between pristine and aged membranes. **Fig. 7c** shows the SANS profiles of HTU hybrid membranes containing 7 wt% SG, measured in 18 % D_2O (HTU phase matched out) after exposure to increasing H_2O_2 concentrations (up to 0.3 %). The corresponding evolution of the ionomer spacing d_{iono}, together with the water uptake and proton conductivity, is reported in **Fig. 7d** as a function of SG content and sPEEK volume fraction. Similarly, **Fig. 7e** presents the SANS profiles of TTU hybrid membranes containing 7 wt% SG, measured in 25 % D_2O under identical aging conditions, with d_{iono} values plotted in **Fig. 7f**.

Upon aging, the ionomer peak shifts toward lower q in both HTU and TTU membranes, indicating an expansion of the ionic domains. d_{iono} increases from 66 to 94 Å (≈ 1.4×) in HTU and from 71 to 84 Å (≈ 1.2×) in TTU. The relative expansions are of the same order, although somewhat larger for HTU, and both remain below that of pristine sPEEK (115 Å, ≈ 1.7×). The slightly larger expansion observed in HTU may reflect partial oxidation of the SG network, effectively reducing the connectivity of the originally hexafunctional network toward a trifunctional-like structure, which partially relaxes the ionic domains.

These structural changes are accompanied by increased water uptake (≈ 3.0× for HTU and 1.3× for TTU at 0.3 % H_2O_2). Importantly, water uptake remains measurable in both hybrid membranes beyond 0.1 % H_2O_2, indicating that the SG phase mitigates over-swelling and preserves the structural integrity of the sPEEK matrix.

Regarding proton conductivity, HTU membranes remain nearly constant (40 → 38 $mS.cm^{-1}$) up to 0.3 % H_2O_2, whereas TTU decreases significantly (59 → 44 $mS.cm^{-1}$) and pristine sPEEK drops sharply (79 → 54 $mS.cm^{-1}$), becoming unmeasurable beyond 0.1 % H_2O_2. These results highlight the superior structural and functional stability of HTU hybrid membranes under oxidative aging, despite their ionic-domain expansion following a trend similar to that of sPEEK.

Taken together, these results highlight the sacrificial function of the thiourea-based SG phase in mitigating oxidative stress, by inhibiting oxidation reactions and thereby preserving the sPEEK matrix and its nanoscale morphology. This protective mechanism limits over-swelling of the ionic domains and prevents dispersion of polymer aggregates, maintaining the nanoscale phase-segregated structure. As a result, both mechanical integrity and proton conductivity are retained under oxidative stress.

(ii) Evolution of the sol-gel phase organization and accessibility under oxidative aging

In the previous sections, the analysis focused on hybrid membranes containing 7 wt% SG, a composition that maintains proton conductivity at levels suitable for fuel cell operation. Here, the study is extended to membranes with higher SG loadings (24 wt% for HTU and 18 wt% for TTU) to facilitate the

Open Access Article. Published on 11 June 2026. Downloaded on 6/12/2026 10:57:08 PM.
This article is licensed under a Creative Commons Attribution 3.0 Unported Licence.

Journal of Materials Chemistry A Accepted Manuscript

View Article Online
DOI: 10.1039/D6TA03128E

observation of structural changes associated with SG consumption during oxidative aging. For clarity, only dry-state membranes are considered, allowing us to isolate the effects of SG degradation from hydration-induced swelling and structural rearrangements.

HTU membranes. Dry-state SANS profiles of HTU membranes containing 7 wt% and 24 wt% SG were recorded following exposure to increasing H_2O_2 concentrations, as shown in **Fig. 8a** and **8b**, respectively.

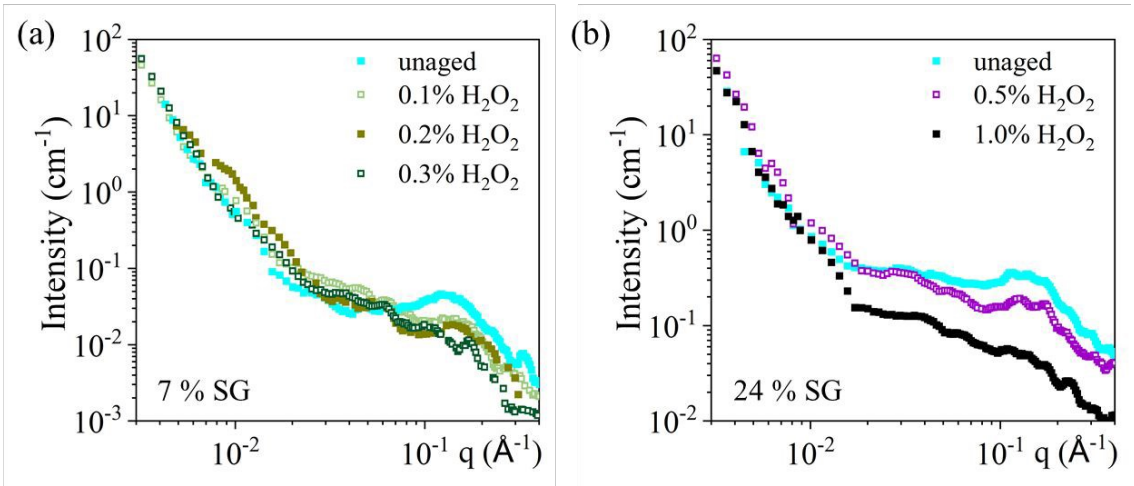

Fig. 8. Dry-state SANS profiles of HTU hybrid membranes: (a) 7 wt% SG and (b) 24 wt% SG after ageing in H_2O_2 solutions at different concentrations (0% (unaged reference), 0.1-0.3% for 7 wt% and 0.5–1% for 24 wt%). The "unaged" samples correspond to membranes subjected to the same protocol as the aged samples, but without oxidant exposure (blank reference): 24 h in water at 80 °C, followed by drying.

In HTU membranes, the intensity of the hybrid peak gradually decreases with increasing H_2O_2 concentration, reflecting the progressive consumption of SG confined within the ionic channels. This effect is particularly pronounced in the 24 wt% HTU membrane, whose higher SG content produces a stronger scattering signal. The relatively low water uptake (39 % vs. 153 % for 7 wt% SG) likely limits the access of reactive species, slowing degradation. Consequently, dry-state scattering profiles remain measurable even after exposure to H_2O_2 concentrations up to 1 %.

In the 7 wt% HTU membrane, the hybrid peak persists up to 0.2% H_2O_2, consistent with the preservation of proton conductivity over the same range. In this regime, total protection is provided by the highly reactive thiourea groups confined within the ionic channels, fully inhibiting oxidation of the sPEEK backbone. As long as the SG phase persists within the ionic domains, nanoscale morphology, macromolecular integrity, and proton transport are preserved. Once the SG phase begins to be consumed, secondary protection limits the rate of oxidation of the sPEEK matrix, which proceeds more slowly than in pristine sPEEK. Formation of carboxylic acid groups (observed via an IR band at 1735 cm^{-1} [64,65]) increases local hydrophilicity, leading to higher water uptake and a shift of the ionomer peak toward lower q values, reflecting enhanced swelling of the ionic domains.

Open Access Article. Published on 11 June 2026. Downloaded on 6/12/2026 10:57:08 PM.
This article is licensed under a Creative Commons Attribution 3.0 Unported Licence.

Journal of Materials Chemistry A Accepted Manuscript

View Article Online
DOI: 10.1039/D6TA03128E

TTU membranes. Dry-state SANS profiles of TTU hybrid membranes containing 18 wt% SG were recorded following exposure to increasing H_2O_2 concentrations (**Fig. 9**).

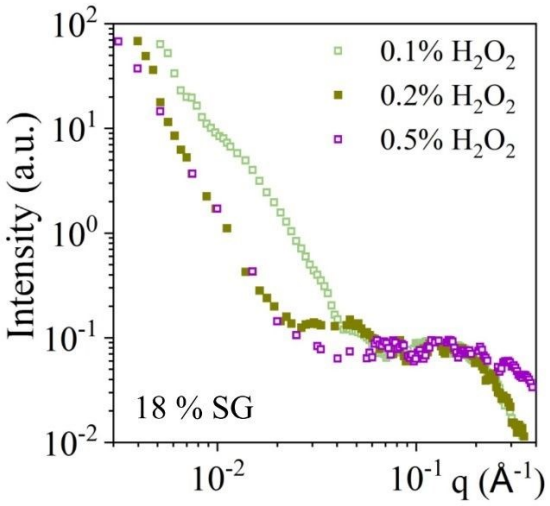

Fig. 9. Dry-state SANS profiles of TTU hybrid membranes containing 18 wt% SG after aging in 0.1, 0.2 and 0.5 % H_2O_2.

A two-step behavior is observed in TTU membranes. Up to 0.1% H_2O_2, scattering from the interbundle regions is preserved, indicating that the SG phase located in these regions is not significantly consumed by oxidation. The absence of oxidation of the sPEEK phase[65] therefore results from the preferential consumption of oxidizing species by the SG phase confined within the ionic channels (see **Fig. 4b**), where oxidizing species are preferentially transported through water-filled pathways.

At 0.1% H_2O_2, the hybrid peak is hardly observed, indicating the strong decrease of the SG/sPEEK contrast within the ionic channels. Between 0.1 and 0.2% H_2O_2, the decrease in the signal associated with the interbundle regions reflects the progressive consumption of antioxidant functions located in these areas, which are necessarily less reactive than those confined within the ionic domains and more directly exposed to oxidizing species. This marks the transition from total to secondary protection, governed by differences in the reactivity of antioxidant functions depending on their proximity to oxidizing species transported by water within the ionic network.[65]

A different behavior is observed for HTU-based membranes. Beyond 0.1% H_2O_2, corresponding to the end of the total protection regime, the hybrid peak remains observable despite the consumption of the antioxidant SG phase within the ionic channels. This behavior suggests that, although the antioxidant functionalities have been consumed, the polysiloxane skeleton itself remains present within the ionic network. Owing to the highly crosslinked nature of the HTU-derived SG phase, related to the hexafunctional character of the precursor, sufficient SG/sPEEK contrast is therefore maintained to preserve the hybrid peak.

In contrast, for TTU-based membranes, the disappearance of the hybrid peak at 0.1% H_2O_2 suggests that the consumption of the antioxidant functionalities is accompanied by the elution or loss of the SG phase from the ionic channels. As TTU is a trifunctional precursor, the resulting SG network is less crosslinked

Open Access Article. Published on 11 June 2026. Downloaded on 6/12/2026 10:57:08 PM.
This article is licensed under a Creative Commons Attribution 3.0 Unported Licence.

Journal of Materials Chemistry A Accepted Manuscript

View Article Online
DOI: 10.1039/D6TA03128E

and therefore less structurally retained within the ionic domains, leading to the disappearance of the SG/sPEEK scattering contrast and thus of the hybrid peak.

4. CONCLUSION

This study provides a structure-driven understanding of how thiourea-functionalized sol-gel (SG) phases enhance the oxidative stability of sPEEK hybrid membranes. While TEM and AFM show no discrete domains, SANS reveals nanoscale density fluctuations arising from SG confined within ionic channels (hybrid peak) and SG intimately mixed with sPEEK chains in interbundle regions.

HTU and TTU precursors generate distinct morphologies.

In HTU membranes, SG incorporation within the ionic channels increases at low SG contents before reaching a regime where additional SG is preferentially located in interbundle regions. These interbundle regions contain ~5 nm SG/sPEEK domains whose number increases with SG loading, while hydration primarily expands the spacing between SG regions in the channels.

In TTU membranes, SG incorporation within the ionic channels remains nearly constant, whereas, ~20 nm interbundle SG/sPEEK domains reorganize with increasing SG content, suggesting a phase-inversion-like behavior: at low SG loading, SG domains are embedded in a continuous sPEEK matrix, whereas at high SG loading, sPEEK domains become dispersed within an SG-rich phase.

At low SG contents (<10 wt%), the number of condensable groups carried by the precursors has only a limited impact on the macroscopic membrane properties, since the SG phase is mainly confined within the ionic domains. In the absence of a significant amount of SG phase within the interbundle regions, the effects on membrane swelling and therefore on macroscopic properties such as water uptake and proton conductivity remain limited. At higher SG contents, however, the growth of the SG phase within the interbundle regions increasingly affects the physical properties of the membrane. These effects become more pronounced as both the SG content and the crosslinking degree of the SG phase increase. More specifically, the HTU precursor, owing to its hexafunctional character, forms a denser and more highly crosslinked SG network, resulting in stronger rigidification effects and lower water uptake, whereas TTU generates a less crosslinked SG phase, preserving higher membrane hydration and proton transport properties.

Increasing SG content leads to a reduction in water uptake and proton conductivity. However, in HTU membranes, this decrease is primarily governed by the highly crosslinked hexafunctional nature of the SG network rather than by SG content alone. Importantly, proton conductivity remains compatible with fuel cell operation (~50 $mS.cm^{-1}$) up to about 7-10 wt% SG, indicating that ion transport is preserved despite the morphological evolution.

Under oxidative stress, thiourea groups act as sacrificial species, protecting the sPEEK backbone. The structural evolution of the membranes reveals a two-step protective mechanism governed by the spatial distribution of the SG phase within the ionic morphology. Total protection is provided by SG confined

Open Access Article. Published on 11 June 2026. Downloaded on 6/12/2026 10:57:08 PM.
This article is licensed under a Creative Commons Attribution 3.0 Unported Licence.

Journal of Materials Chemistry A Accepted Manuscript

View Article Online
DOI: 10.1039/D6TA03128E

within the ionic domains, where oxidizing species are preferentially transported through water-filled pathways, while secondary protection originates from SG located in interbundle regions. This sequential protection mechanism is observed independently of the chemistry of the SG precursors and therefore appears to be primarily governed by the spatial localization of the SG phase within the membrane morphology.

In contrast, the functional properties of the membranes, including proton conductivity and hydration behavior, are mainly governed by the chemistry and functionality of the SG precursors through their influence on the organization of the ionic network and on the crosslinking density of the SG phase.

Once the protective SG populations are consumed, oxidation of the hydrocarbon matrix leads to the formation of carboxylic acid groups, increased membrane hydrophilicity, enhanced water uptake, and greater swelling of the ionic domains. HTU membranes outperform both TTU and pristine sPEEK under ex situ aging and fuel cell operating conditions (258 h vs. 192 h and 144 h, respectively),[65] highlighting the critical role of SG nanoscale organization in controlling membrane durability.

Overall, these findings demonstrate that oxidative protection in PEMFC membranes depends not only on the presence of thiourea-functionalized SG phases, but also on their spatial localization and accessibility within the ionic network, providing new design guidelines for durable hybrid PEMs.

AUTHORS CONTRIBUTION

Claire Tougne: Investigation, Data curation, Formal analysis, Writing – original draft, Writing – review & editing.

Meriem Daoudi: Fuel cell tests.

Evelise Ferri: Membrane synthesis.

Vincent H. Mareau: Funding acquisition, Writing – review & editing.

Véronique Dufaud: Writing – review & editing.

Catherine Santini: Writing – review & editing.

Eliane Espuche: Writing – review & editing.

Olivier Lottin: Writing – review & editing.

Jean-Christophe Perrin: Writing – review & editing.

Jérôme Dillet: Fuel cell tests, Writing – review & editing.

Assma El Kaddouri: Writing – review & editing.

Lionel Porcar: Formal analysis (SANS).

Laurent Gonon: Funding acquisition, Supervision, Writing – review & editing.

Hakima Mendil-Jakani: Funding acquisition, Supervision, Conceptualization, Formal analysis, Writing – original draft, Writing – review & editing.

ACKNOWLEDGEMENTS

Open Access Article. Published on 11 June 2026. Downloaded on 6/12/2026 10:57:08 PM.
This article is licensed under a Creative Commons Attribution 3.0 Unported Licence.

Journal of Materials Chemistry A Accepted Manuscript

View Article Online
DOI: 10.1039/D6TA03128E

This work was supported by the French National Research Agency (project ANR-18-CE05-0027 MULTISTABLE). The authors acknowledge the Institut Laue-Langevin (ILL) for the allocation of beamtime on D22 (exp. 6-07-72) and for technical support during the experiments. Raw data are available in accordance with the ILL data policy at: https://doi.ill.fr/10.5291/ILL-DATA.6-07-72.

NOTES

The authors declare no competing financial interest.

REFERENCES

1 Clean Hydrogen Partnership, *Strategic Research and Innovation Agenda 2021 – 2027*, 2022.

2 J. Marcinkoski, R. Vijayagopal, J. Adams, B. James, J. Kopasz and R. Ahluwalia, *DOE Advanced Truck Technologies Subsection of the Electrified Powertrain Roadmap Technical Targets for Hydrogen-Fueled Long-Haul Tractor-Trailer Trucks*, 2019.

3 S. J. Osborn, M. K. Hassan, G. M. Divoux, D. W. Rhoades, K. A. Mauritz and R. B. Moore, *Macromolecules*, 2007, **40**, 3886–3890.

4 F. Bauer, S. Denneler and M. Willert-Porada, *J. Polym. Sci. Part B Polym. Phys.*, 2005, **43**, 786–795.

5 M. Zatoń, J. Rozière and D. J. Jones, *Sustain. Energy Fuels*, 2017, **1**, 409–438.

6 A. Kusoglu and A. Z. Weber, *J. Phys. Chem. Lett.*, 2015, **6**, 4547–4552.

7 X. Yu, S. Bai, Q. Li, Z. Zhao, Q. Sun, S. Cao, H. Cui, M. Liu, Q. Xu and C.-C. Hou, *EnergyChem*, 2025, **7**, 100142.

8 Z. Rui and J. Liu, *Prog. Nat. Sci. Mater. Int.*, 2020, **30**, 732–742.

9 E. Quartarone, S. Angioni and P. Mustarelli, *Materials (Basel).*, 2017, **10**, 687.

10 B. Campagne, G. David, B. Ameduri, D. J. Jones, J. Rozière and I. Roche, *Int. J. Hydrogen Energy*, 2015, **40**, 16797–16813.

11 V. Delhorbe, S. R. Reijerkerk, C. Cailleteau, M. Bathfield, L. Chikh, F. Gouanve, L. Ogier, E. Espuche, B. Ameduri, S. Vidal, G. Gebel, A. Morin and O. Fichet, *J. Memb. Sci.*, 2013, **429**, 168–180.

12 E. Qu, M. Xiao, D. Han, S. Huang, Z. Huang, W. Liu, S. Wang and Y. Meng, *Nanomaterials*, 2023, **13**, 266.

13 H. Hu, M. Gopinadhan and C. O. Osuji, *Soft Matter*, 2014, **10**, 3867–3889.

14 S. Swaby, N. Ureña, M. Teresa Pérez-Prior, C. del Río, A. Várez, J. Y. Sanchez, C. Iojoiu and B. Levenfeld, *J. Ind. Eng. Chem.*, 2023, **122**, 366–377.

15 F. Wijaya, S. Woo, H. Lee, A. F. Nugraha, D. Shin and B. Bae, *J. Memb. Sci.*, 2022, **645**, 120203.

16 A. Pokprasert, P. Theato and S. Chirachanchai, *Polymer (Guildf).*, 2022, **240**, 124523.

17 M. J. Parnian, S. Rowshanzamir and F. Gashoul, *Energy*, 2017, **125**, 614–628.

Open Access Article. Published on 11 June 2026. Downloaded on 6/12/2026 10:57:08 PM.
This article is licensed under a Creative Commons Attribution 3.0 Unported Licence.

Journal of Materials Chemistry A Accepted Manuscript

View Article Online
DOI: 10.1039/D6TA03128E

18 E. van Keulen, S. J. M. C. Bouwman, S. Pikavet and A. Asadi Tashvigh, *Energy and Fuels*, 2026, **40**, 6606–6637.

19 Y. Zhou, B. Wang, Z. Ling, Q. Liu, X. Fu, Y. Zhang, R. Zhang, S. Hu, F. Zhao, X. Li, X. Bao and J. Yang, *Sci. Total Environ.*, 2024, **921**, 171099.

20 Q. Liu, B. Wang, Z. Ling, Y. Zhou, S. Hu, X. Fu, R. Zhang, Y. Zhang, F. Zhao, X. Li, N. Li and J. Yang, *Nano Energy*, 2025, **139**, 110980.

21 M. Tanaka, Y. Takeda, T. Wakiya, Y. Wakamoto, K. Harigaya, T. Ito, T. Tarao and H. Kawakami, *J. Power Sources*, 2017, **342**, 125–134.

22 S. Shi, A. Z. Weber and A. Kusoglu, *J. Memb. Sci.*, 2016, **516**, 123–134.

23 T. Kwon, Y. Lim, J. Cho, R. Lawler, B. J. Min, W. A. Goddard, S. S. Jang and J. Y. Kim, *Mater. Today*, 2022, **58**, 135–163.

24 H. Huang, X. Zhang, J. Fan, H. Li and H. Wang, *Int. J. Hydrogen Energy*, 2022, **47**, 18109–18121.

25 T. Agarwal, I. Matanovic, S. Adhikari, E. J. Park, S. Komini Babu, Y. S. Kim, D. Tian, C. Bae, O. Morales-Collazo, J. F. Brennecke, A. K. Prasad, S. G. Advani, A. Sievert, T. Hopkins, A. Park and R. Borup, *J. Power Sources*, 2023, **554**, 232320.

26 S. Wang, M. Yan, Y. Li, C. Vinado and J. Yang, *J. Power Sources*, 2018, **393**, 75–82.

27 D. Shin, M. Han, Y. G. Shul, H. Lee and B. Bae, *J. Power Sources*, 2018, **378**, 468–474.

28 X. Liu, Y. Li, M. Li, N. Xie, J. Zhang, Y. Qin, Y. Yin and M. D. Guiver, *J. Memb. Sci.*, 2021, **629**, 119282.

29 P. P. Sharma and D. Kim, *Membranes (Basel).*, 2022, **12**, 521.

30 L. Liu, Y. Li, R. Qiao, Y. Xing and H. Li, *Energy & Fuels*, 2021, **35**, 12482–12494.

31 H. Huang, S. Xu, J. Zhou, F. Luo, J. Fan and H. Li, *J. Memb. Sci.*, 2021, **636**, 119614.

32 D. C. T. Vo, M. D. T. Nguyen and D. Kim, *Mol. Syst. Des. Eng.*, 2019, **4**, 901–911.

33 S. Zhao, Y. Liao, R. Wang, Y. Li, J. Shuai, L. Wang, B. Liu, R. Chen, T. Tian, H. Zhang and H. Tang, *Adv. Compos. Hybrid Mater.*, 2024, **7**, 66.

34 M. Zatoń, B. Prélot, N. Donzel, J. Rozière and D. J. Jones, *J. Electrochem. Soc.*, 2018, **165**, F3281–F3289.

35 A. M. Baker, A. R. Crothers, K. Chintam, X. Luo, A. Z. Weber, R. L. Borup and A. Kusoglu, *ACS Appl. Polym. Mater.*, 2020, **2**, 3642–3656.

36 S. Yang and D. Kim, *J. Power Sources*, 2018, **393**, 11–18.

37 M. Zatoń, J. Rozière and D. J. Jones, *J. Mater. Chem. A*, 2017, **5**, 5390–5401.

38 A. M. Baker, L. Wang, W. B. Johnson, A. K. Prasad and S. G. Advani, *J. Phys. Chem. C*, 2014, **118**, 26796–26802.

39 D. Banham, S. Ye, T. Cheng, S. Knights, S. M. Stewart, M. Wilson and F. Garzon, *J. Electrochem. Soc.*, 2014, **161**, F1075–F1080.

40 M. T. Taghizadeh and M. Vatanparast, *RSC Adv.*, 2016, **6**, 56819–56826.

Open Access Article. Published on 11 June 2026. Downloaded on 6/12/2026 10:57:08 PM.
This article is licensed under a Creative Commons Attribution 3.0 Unported Licence.

Journal of Materials Chemistry A Accepted Manuscript

View Article Online
DOI: 10.1039/D6TA03128E

41 L. Liu, Y. Xing, Y. Li, Z. Fu, Z. Li and H. Li, *ACS Appl. Energy Mater.*, 2022, **5**, 8743–8755.

42 T. Kwon, S. H. Park, B. J. Min, S. Park, S. Ramadhani, Y. Lim, S. S. Jang, H. Jeong, H. J. Son and J. Y. Kim, *Adv. Energy Sustain. Res.*, 2022, **3**, 2200011.

43 C. Zheng, N. Xie, X. Liu, L. Wang, W. Zhu, Y. Pei, R. Yue, H. Liu, S. Yin, J. Yao, J. Zhang, Y. Yin and M. D. Guiver, *J. Memb. Sci.*, 2024, **690**, 122195.

44 Y. S. Kang, S. Jang, E. Choi, S. Jo, S. M. Kim and S. J. Yoo, *Int. J. Energy Res.*, 2022, **46**, 6457–6470.

45 F. Bu, Y. Zhang, L. Hong, W. Zhao, D. Li, J. Li, H. Na and C. Zhao, *J. Memb. Sci.*, 2018, **545**, 167–175.

46 H. Huang, X. Zeng, X. Zhang, J. Fan and H. Li, *J. Power Sources*, 2023, **558**, 232602.

47 S. Zhao, Y. Liao, R. Wang, G. Liu, H. Zhang and H. Tang, *Chem. Eng. J.*, 2023, **472**, 144804.

48 K. Xu, S. Pei, W. Zhang, Z. Han, P. Guan, L. Wang, Y. Zou, H. Ding, X. Ma, C. Xu, F. Liu and Y. Zhang, *Mater. Today Energy*, 2023, **31**, 101195.

49 T. de Wild, T. Nemeth, P. Becker, D. Günther, T. Nauser, T. J. Schmidt and L. Gubler, *J. Power Sources*, 2023, **560**, 232525.

50 P. A. Yurova, V. R. Malakhova, E. V. Gerasimova, I. A. Stenina and A. B. Yaroslavtsev, *Polymers (Basel).*, 2021, **13**, 2513.

51 X. Shen, X. Liang, Y. Xu, W. Yu, Q. Li, X. Ge, L. Wu and T. Xu, *J. Memb. Sci.*, 2023, **675**, 121556.

52 J. Wang, Y. Dai, R. Wan, W. Wei, S. Xu, F. Zhai and R. He, *Chem. Eng. J.*, 2021, **413**, 127541.

53 S. H. Yook, H. Y. Kim, S. J. Kim, S. Choi, T. Kwon, H. Cho, J. M. Kim, K. R. Yoon, S. Jo, S. Y. Lee, H. J. Kim, H. J. Son, K. H. Chae, J. Kim, K. Y. Lee and J. Y. Kim, *Chem. Eng. J.*, 2022, **432**, 134419.

54 A. Martinez-Gomez, I. Caballero and C. A. Blanco, *Biomolecules*, 2020, **10**, 400.

55 M. Bredács, E. Kanatschnig, A. Frank, G. Oreski, G. Pinter and S. Gergely, *Polym. Degrad. Stab.*, 2023, **212**, 110345.

56 J. Park, Y. Park and D. Kim, *J. Polym. Sci. Part A Polym. Chem.*, 2019, **57**, 101–109.

57 B. Liu, Y. Duan, Y. Pang, Q. Li and C. Zhao, *Chem. Eng. J.*, 2023, **477**, 146955.

58 S. Park, H. Lee, S.-H. Shin, N. Kim, D. Shin and B. Bae, *ACS Omega*, 2018, **3**, 11262–11269.

59 X. Li, X. Chen, X. Guo, J. Fang, H. Li and B. Wang, *Int. J. Hydrogen Energy*, 2024, **61**, 473–480.

60 K. Kim, J. Bae, M. Y. Lim, P. Heo, S. W. Choi, H. H. Kwon and J. C. Lee, *J. Memb. Sci.*, 2017, **525**, 125–134.

61 Y. Pang, Y. Duan, Q. Li, B. Liu, X. Hu, Q. Liu and C. Zhao, *J. Memb. Sci.*, 2023, **686**, 121999.

62 N. Huynh, J. P. C. Fernandes, P. A. Bayle, M. Bardet, E. Espuche, J. Dillet, J. C. Perrin, A. El Kaddouri, O. Lottin, V. H. Mareau, H. Mendil-Jakani and L. Gonon, *J. Power Sources*, 2020, **462**, 228164.

Open Access Article. Published on 11 June 2026. Downloaded on 6/12/2026 10:57:08 PM.
This article is licensed under a Creative Commons Attribution 3.0 Unported Licence.

Journal of Materials Chemistry A Accepted Manuscript

View Article Online
DOI: 10.1039/D6TA03128E

63 N. Huynh, J. P. Cosas Fernandes, V. H. Mareau, L. Gonon, S. Pouget, P. H. Jouneau, L. Porcar and H. Mendil-Jakani, *Nanoscale Adv.*, 2021, **3**, 2567–2576.

64 C. Tougne, PhD thesis, Université Grenoble Alpes, 2023.

65 C. Tougne, M. Daoudi, E. Ferri, V. H. Mareau, H. Mendil-Jakani, V. Dufaud, C. Santini, E. Espuche, O. Lottin, J. C. Perrin, J. Dillet, A. El Kaddouri and L. Gonon, *Electrochim. Acta*, 2025, **541**, 147338.

66 S. H. Shin, A. Kodir, D. Shin, S. H. Park and B. Bae, *Electrochim. Acta*, 2019, **298**, 901–909.

67 A. Kodir, S. H. Shin, S. Park, M. R. Arbi, T. H. Yang, H. Lee, D. Shin and B. Bae, *Int. J. Energy Res.*, 2022, **46**, 7186–7200.

68 Y. Huo, Q. Li, Z. Rui, R. Ding, J. Liu, J. Li and J. Liu, *J. Memb. Sci.*, 2021, **635**, 119453.

69 T. Agarwal, S. Adhikari, Y. S. Kim, S. Komini Babu, D. Tian, C. Bae, N. N. T. Pham, S. G. Lee, A. K. Prasad, S. G. Advani, A. Sievert, W. P. Rasika Liyanage, T. E. Hopkins, A. Park and R. Borup, *J. Mater. Chem. A*, 2023, **11**, 9748–9754.

70 H. Kim, S. H. Yook, H. Y. Kim, Y. Choi, Y. Lim, Y. Hwang, J. Kim, K. Y. Lee, S. S. Jang, J. Park and J. Y. Kim, *Adv. Electron. Mater.*, 2022, **8**, 2200171.

71 B. Barik, B. Singh, Y. Namgung, M. S. Islam, M.-K. Han, J.-Y. Park and S.-J. Song, *J. Electrochem. Soc.*, 2024, **171**, 074501.

72 G. Monin, PhD thesis, Université de Grenoble, 2012.

73 F. Lu, X. Dong, J. He, C. Hu, W. Chen, S. Hu, Y. Liu, Q. Liu, X. Fu, H. Tan and A. Huang, *J. Polym. Res.*, DOI:10.1007/S10965-025-04433-W.

74 D. Huang, X. Li, C. Luo, P. Wei, Y. Sui, J. Wen, C. Cong, X. Zhang, X. Meng and Q. Zhou, *J. Memb. Sci.*, 2022, **662**, 121001.

75 L. Li, Y. Wang, F. Li, J. Zhao, B. Su, X. Wang, L. Shi, J. Mu, Y. Wang, P. Li and X. Zhang, *Int. J. Hydrogen Energy*, 2024, **72**, 9–19.

76 K. A. Mauritz, *Mater. Sci. Eng. C*, 1998, **6**, 121–133.

77 K. A. Mauritz and M. K. Hassan, *Polym. Rev.*, 2007, **47**, 543–565.

78 A. G. Kannan, N. R. Choudhury and N. K. Dutta, *J. Memb. Sci.*, 2009, **333**, 50–58.

79 C. M. Branco, S. Sharma, M. M. De Camargo Forte and R. Steinberger-Wilckens, *J. Power Sources*, 2016, **316**, 139–159.

80 K. D. Kreuer and G. Portale, *Adv. Funct. Mater.*, 2013, **23**, 5390–5397.

81 H. Mendil-Jakani, I. Zamanillo López, V. H. Mareau and L. Gonon, *Phys. Chem. Chem. Phys.*, 2017, **19**, 16013–16022.

82 E. Machado Ferri da Silva, PhD thesis, Université Claude Bernard - Lyon I, 2023.

83 E. Ferri, C. Tougne, M. Daoudi, F. Gouanvé, O. Gain, L. Gonon, V. H. Mareau, H. Mendil-Jakani, A. El Kaddouri, J. C. Perrin, J. Dillet, O. Lottin, C. C. Santini, E. Espuche and V. Dufaud, *React. Funct. Polym.*, 2026, **219**, 106588.

84 M. Arifoglu, W. N. Marmer and R. L. Dudley, *Text. Res. J.*, 1992, **62**, 94–100.

Open Access Article. Published on 11 June 2026. Downloaded on 6/12/2026 10:57:08 PM.
This article is licensed under a Creative Commons Attribution 3.0 Unported Licence.

Journal of Materials Chemistry A Accepted Manuscript

View Article Online
DOI: 10.1039/D6TA03128E

85 S. Sahu, P. Rani Sahoo, S. Patel and B. K. Mishra, *J. Sulfur Chem.*, 2011, **32**, 171–197.

86 M. Hoffmann and J. O. Edwards, *Inorg. Chem.*, 1977, **16**, 3333–3338.

87 H. Mendil-Jakani, I. Zamanillo López, P. M. Legrand, V. H. Mareau and L. Gonon, *Phys. Chem. Chem. Phys.*, 2014, **16**, 11243–11250.

88 M. Daoudi, E. Ferri, C. Tougne, A. El Kaddouri, J. C. Perrin, J. Dillet, L. Gonon, V. Mareau, H. Mendil-Jakani, V. Dufaud, E. Espuche and O. Lottin, *J. Polym. Sci.*, 2023, **61**, 761–776.

89 R. S. Waremra and P. Betaubun, *E3S Web Conf.*, 2018, **73**, 13019.

90 J. P. Cosas Fernandes, V. H. Mareau and L. Gonon, *Polymer (Guildf).*, 2018, **137**, 231–244.

91 E. M. Davis, J. Kim, V. P. Oleshko, K. A. Page and C. L. Soles, *Adv. Funct. Mater.*, 2015, **25**, 4064–4075.

92 L. Rubatat, G. Gebel and O. Diat, *Macromolecules*, 2004, **37**, 7772–7783.

93 O. Glatter and O. Kratky, *Small Angle X-ray Scattering*, Academic Press, London, 1982.

94 C. Perrot, G. Meyer, L. Gonon and G. Gebel, *Fuel Cells*, 2006, **6**, 10–15.

Open Access Article. Published on 11 June 2026. Downloaded on 6/12/2026 10:57:08 PM.
This article is licensed under a Creative Commons Attribution 3.0 Unported Licence.

Journal of Materials Chemistry A Accepted Manuscript

- The data supporting this article have been included as part of the Supplementary Information.

View Article Online
DOI: 10.1039/D6TA03128E

Open Access Article. Published on 11 June 2026. Downloaded on 6/12/2026 10:57:08 PM.
This article is licensed under a Creative Commons Attribution 3.0 Unported Licence.

Journal of Materials Chemistry A Accepted Manuscript